ASBESTOS DETECTION IN CONSTRUCTION AND DEMOLITION WASTE ADOPTING DIFFERENT CLASSIFICATION APPROACHES BASED ON SHORT WAVE INFRARED HYPERSPECTRAL IMAGING

Giuseppe Bonifazi [1,*], Giuseppe Capobianco [1], Silvia Serranti [1], Sergio Malinconico [2] and Federica Paglietti [2]

[1] Department of Chemical Engineering, Materials and Environment, Sapienza University of Rome, Italy
[2] Department of new technologies for occupational safety of industrial plants, products and anthropic settlements, National Institute for Insurance against Accidents at Work, Rome, Italy

ABSTRACT

Asbestos has been widely used in many applications for its technical properties (i.e. resistance to abrasion, heat and chemicals). Despite its properties, asbestos is recognized as a hazardous material to human health. In this paper a study, based on multivariate analysis, was carried out to verify the possibilities to utilize the hyperspectral imaging (HSI), working in the short-wave infrared range (SWIR: 1000-2500 nm), to detect the presence of asbestos-containing materials (ACM) in construction and demolition waste (CDW). Multivariate classification methods including classification and regression tree (CART), partial least squares-discriminant analysis (PLS-DA) and correcting output coding with support vector machines (ECOC-SVM), were adopted to perform the recognition/classification of ACM in respect of the other fibrous panels not containing asbestos, in order to verify and compare Efficiency and robustness of the classifiers. The correctness of classification results was confirmed by micro-X-ray fluorescence maps. The results demonstrate as SWIR technology, coupled with multivariate analysis modeling, is a quite promising approach to develop both "off-line" and "on-line" fast reliable and robust quality control strategies, finalized to perform a first evaluation of the presence of ACM.

1. INTRODUCTION

Asbestos is the common name used for two families of fibrous minerals of different crystallographic and chemical characteristics: serpentine (i.e. chrysotile: $Mg_3(Si_2O_5)(OH)_4$) and amphiboles (e.g. crocidolite: $Na_2(Fe^{2+}_3Fe^{3+}_2)Si_8O_{22}(OH)_2$ and amosite: $Fe_7Si_8O_{22}(OH)_2$) (NIOSH, 2008). Asbestos has been widely used in many applications for its technical properties, for its resistance to abrasion, heat and chemicals (NIOSH, 2008). In the past, common asbestos construction materials were duct and pipe insulation, cement, siding, flooring, roofing, and in sealants, caulks, and glazes, throughout the 20th century, until it was partially banned in different world countries (Allen et al., 2018). In addition, many natural minerals that may be classified as asbestos are common constituent in many regions of every continent, of some rocks and soils, (Gualtieri, 2020). Despite its properties, asbestos is recognized as a hazardous material to human health and since 1980 it has been banned in many industrialized countries. The exposure of people to asbestos is quite huge. The World Health Organ-

ization (WHO) report shows that about 125 million people are exposed to asbestos at the workplace. Every year, asbestos-related-tumors produce the death of about 100,000 people, of which several thousand related to asbestos exposure at home. In this scenario, asbestos-containing materials (ACM) identification techniques are crucial for environmental control in contaminated areas such as the proximity of asbestos mines and factories or industrial sites (Colangelo et al., 2011). A site contaminated with asbestos can be reclaimed through removal, encapsulation, or confinement (Gualtieri, 2020). If ACM were removed, a careful monitoring plan to verify the "residual" presence of asbestos is necessary (Tomasetti et al., 2020). The possibility to implement fast and reliable analytical methods to detect and identify asbestos fibers not only at laboratory scale, but also to develop and apply analytical methods directly working "in situ" is of great interest in terms of safety, time and costs. The main analytical techniques for asbestos recognition (i.e., Fourier transform infrared spectroscopy (FT-IR), polarized light microscopy (PLM), X-ray diffraction and scanning electron microscopy (SEM)

and μ-Raman spectroscopy allow to recognize micrometric asbestos fibers. However, they require the physical collection and preparation of samples and usually allow the performance of punctual measurements and small area mapping (Stănescu-Dumitru, R., 2008; Petriglieri et al, 2011; Gandolfi et al, 2016). Hyperspectral imaging (HSI) is a non-destructive technique, combining imaging with spectroscopy. It can represent an important step forward permitting to investigate ACM without any sample preparation (Bonifazi et al., 2018; Bonifazi et al., 2019). This technique provides spectral and spatial information of the sample, thus allowing qualitative and quantitative analysis of the different components occurring in the analyzed material. HSI, coupled with chemometric methods, allows the gathering of information on the characteristics of the investigated materials and their nature, enabling the evaluation of chemical attributes of the sample exposed surface, thanks to the already mentioned 3D nature (i.e. spectral and spatial) of hyperspectral data (Serranti & Bonifazi, 2016). Research activity has demonstrated the possibility to recognize through HSI devices different classes of material inside demolition wastes (Trotta et al., 2021, Bonifazi et al., 2018, Bonifazi et al., 2019,), including ACM (Bonifazi et al., 2019). Furthermore, the use of "in situ" techniques based on HSI could represent a useful tool for the first qualitative identification of materials and/or products containing asbestos fibers. Several studies demonstrate as in the region between 1000 and 2500 nm, most types of asbestos fibers are characterized by a distinct fingerprint related to absorption bands corresponding to the first harmonic of the elongation vibrations O–H (Zholobenko et al., 2021, Cheng et al., 2017, Bonifazi et al., 2018). The remarkable Sensitivity of this technique can be linked to the high anharmonicity of the O–H vibrations and a substantial sampling depth (Lewis et al., 1996). Other investigations showed as asbestos fibers and ACM detection, following a point or a hyperspectral imaging-based approach, reach a detection limit of 0.1 wt% (Zholobenko et al., 2021). The results achieved in this work are in agreement with those published in these studies, showing an Efficiency in the identification of the 3 asbestos fibers and matrix without asbestos close to 1. However, in order to obtain higher Efficiency for different C&DW materials, it is necessary to collect and analyze a larger number of ACM and C&DW samples in order to reduce the presence of false positives (Bonifazi et al., 2019). Furthermore, to improve detection accuracy and to reduce noise effects, different pre-processing strategies should be further explored, being the pre-processing, an important step significantly influencing final results of hyperspectral data (Neo et al., 2022). In detail, through a resolution of 30 microns / pixel it is possible to identify the of asbestos bundles fibers (Bonifazi et al., 2018.), while with a pixel resolution greater than 600 microns, it is possible to qualitatively identify ACMs from non-contaminated materials (Bonifazi et al., 2019). The present work, in terms of methodological approach, aims to apply and compare different pixel-based classification techniques in order to find the most accurate and reliable strategy for asbestos detection through HSI technique. The study was carried out on a set of previously characterized samples, representative of the most common used asbestos minerals. The acquired hyperspectral data were first explored by Principal Component Analysis (PCA). Three different classification models, that is: Partial Least Square-Discriminant Analysis (PLS-DA), Classification And Regression Trees (CART) and Error-Correcting Output Codes integrated with Support Vector Machines (ECOC-SVM) were then applied and their performances were evaluated in terms of prediction maps and statistical parameters.

2. MATERIALS AND METHODS

2.1 Materials

Four pure asbestos samples (Chrysotile standard intermediate 031G, Chrysotile standard NIEHS plastibest 20, Amosite Standard 312M, Amosite standard NIEHS, Crocidolite standard 5174, Crocidolite from Balangero industrial plant, and 'matrix without asbestos'), provided by National Institute for Insurance against Accidents at Work (INAIL) (Rome, Italy), were analyzed in order to create a calibration and validation set (Figure 1). The samples were sealed up in borosilicate glass Petri cups as showed in Figure 1 (Serranti et al., 2019). Furthermore, three asbestos certified samples constituted by amosite, chrysotile and crocidolite fibers were acquired. Finally, two acquisitions were carried out on different areas of the sample without asbestos, in order to obtain a calibration and a validation dataset. The details of samples composition are summarized in Table 1.

2.2 Equipment and statistical analysis

2.2.1 Hyperspectral imaging system set-up and image acquisition

Image acquisition was carried out using a SisuCHEMA XL™ Chemical Imaging Workstation embedding an ImSpector™ N25E (Specim®, Finland) operating in the SWIR range (1000–2500 nm), coupled with a MCT camera (320 × 240 pixels), equipped with a macro lens. The number of acquired spectral bands is 240, with a spectral resolution of 10 nm. The selected configuration of the object-plane scanner covers a 1 cm field of view (FOV) and the spatial resolution is 30 μm/pixel. A diffused line-illumination unit was adopted optimizing the imaging of various surfaces (Specim, 2015). The working distance between the spectrograph lens and the sample tray plan was 10 cm. A schematic image of the utilized device is shown in Figure 2.

The instrument calibration is performed by recording black and white reference images. A certified standard (Spectralon™) is used. Black image (B) was acquired to remove the dark current effect of the camera sensor. The raw data can be converted into normalized reflectance using Equation (1).

$$I = \frac{(I_0 - B)}{(W - B)} \tag{1}$$

where I is the corrected hyperspectral image, I_0 is the original hyperspectral image, B is the black reference image (~0 reflectance) and W is the white reference image (~1 reflectance). The result of acquisition is constituted by a hyperspectral image, in which each column represents the discrete spectrum values of the corresponding ele-
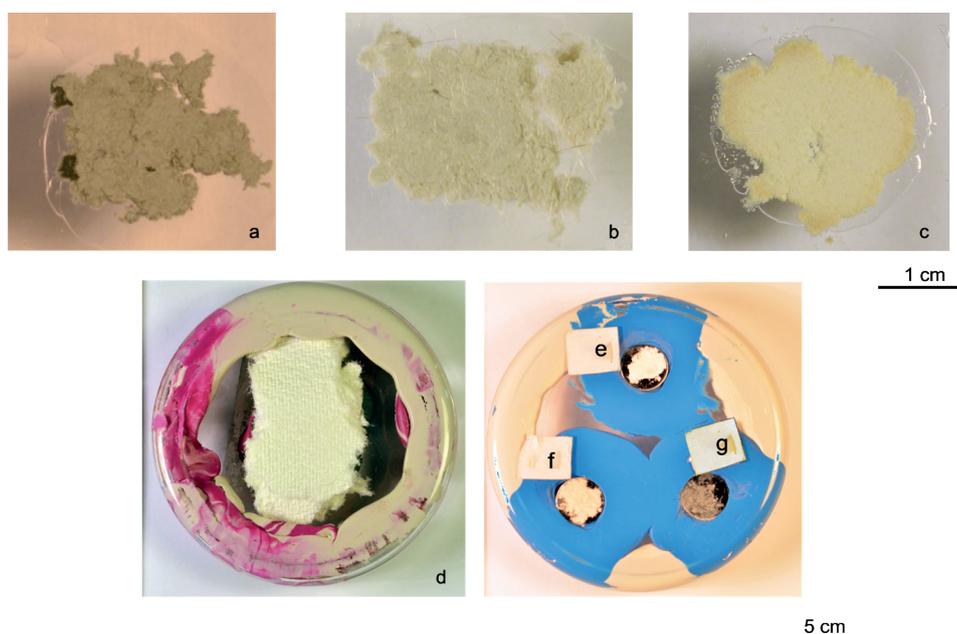
FIGURE 1: RGB image of acquired samples: (a, g) crocidolite, (b, f) amosite, (c, e) chrysotile and (e) panel without asbestos (d).

ments of the sensitive linear array. Asbestos samples were placed on the device scanning table to simulate, at laboratory scale, the handling operative conditions.

2.2.2 Hyperspectral data handling and analysis

The acquired hyperspectral images were analyzed using PLS_Toolbox (Version 8.9 Eigenvector Research, Inc.) (Wise et al., 2006) for PCA and PLS-DA, Statistics and Machine Learning Toolbox™ for CART, ECOC-SVM, all running inside MATLAB® environment (R2019a, Version 8.4, The Mathworks, Inc.). The first step was carried out by PCA to perform background segmentation. In order to process the raw data into PLS_toolbox, HSI-derived spectral data were converted in a 'DataSet object' (DSO), that is a MATLAB® object created to hold both data and metadata (Eigenvector Inc, 2020).

Two mosaic images were created from the acquisitions to divide the acquired data into calibration and validation

TABLE 1: Pure asbestos fiber samples assumed as reference: crocidolite: (a,g), Amosite: (b,f), chrysotile (c,e) and Panel without asbestos (d).

Samples	Detail	Composition
a	Crocidolite standard 5174	$Na_2(Mg, Fe)_6Si_8O_{22}(OH)_2$
b	Amosite Standard 312M	$(Fe^{2+})_2(Fe^{2+}, Mg)_5Si_8O_{22}(OH)_2$
c	Chrysotile standard intermediate 031G	$Mg_3(Si_2O_5) (OH)_4$
d	Dry wall	Main detected elements: Si, S, Cl, K, Ca, Ti, Fe, Zn
e	Chrysotile standard NIEHS plastibest 20	$Mg_3(Si_2O_5) (OH)_4$
f	Amosite standard NIEHS	$(Fe^{2+})_2(Fe^{2+}, Mg)_5Si_8O_{22}(OH)_2)$
g	Crocidolite from Balangero industrial plant	$Na_2(Mg, Fe)_6Si_8O_{22}(OH)_2$

FIGURE 2: A schematic image with a picture of SisuCHEMA XL™ Chemical Imaging Workstation (Specim, Finland).

datasets. After a preliminary data pre-processing, different chemometric methods were then applied: PCA, PLS-DA, CARTECOC-SVM.

Different pre-processing strategies were tested following the combinations widely adopted in literature (Rinnan et al., 2009; Bonifazi et al., 2018). The pre-processing algorithm combination was selected in order to optimize class recognition for the different classification models. In detail, Multipliative Signal Correction (MSC) was chosen to reduce the light scattering effect on the acquired hyperspectral image (Rinnan et al., 2009). The Savitzky–Golay filter was used to perform spectral derivative to reduce additive effects and emphasize the spectral features (Bonifazi et al., 2021). Finally, all data were centered by Mean Center (MC).

PCA is a versatile method enabling an overview of complex multivariate data and it is widely adopted to process HSI data (Amigo, Martì, & Gowen, 2013). This method can be used to reveal relations between variables and samples (i.e., clustering), detecting outliers, evaluating patterns and generating new hypotheses. By using this method, the processed spectral data are decomposed into several principal components (PCs), which are linear combinations of the original spectral data embedding the spectral variations of each collected spectral data set (Bro et al., 2014). According to this approach, a reduced set of factors is produced. Such a set can be used for exploration, since it provides an accurate description of the entire dataset.

PLS-DA is a supervised classification technique requiring prior knowledge of the data. This classification method is used to classify samples into predefined groups by forming discriminant functions from input variables (wavelengths) to yield a new set of transformed values providing more accurate discrimination than any single variable (wavelength) (Ballabio et al., 2013). A discriminant function is then built using pure samples (i.e., samples belonging to known classes) to be later utilized to classify samples belonging to an unknown set.

CART is a non-parametric statistical technique, developed by Breiman et al. (1984) and it is one of the most popular algorithms to build classification and regression trees. CART can solve classification (i.e., categorical dependent variables) as well as regression problems (i.e. continuous dependent variables). In both cases, the method builds a decision tree, describing a response variable as a function of different explanatory variables. The subdivision produces a tree hierarchy, where the observation subsets are the nodes and the final ones are the leaves. In CART, the division that takes place in the nodes is formulated as a binary model in which all the samples satisfying the model are grouped in a subgroup, while the rest in another subgroup (Deconinck et al., 2012).

ECOC-SVM. Support vector machines is a method of machine learning with minimum structure risk, and it is generally employed for classification of two classes (Zheng et al., 2008). It is based on statistical learning theory and was developed by Vapnik in 1995. The primary aim of this technique is to project nonlinear separable samples onto another higher dimensional space by using different types of kernel functions. In recent years, kernel methods have received major attention, especially due to the increased popularity of SVM. Kernel functions play a significant role in SVM to bridge from linearity to nonlinearity (Satapathy et al., 2019). In detail, SVM finds the hyperplane that separates the largest possible fraction of points of the same class on the same side, while maximizing the distance from either class to the hyperplane (Chapelle et al., 1999). Support vector machine (SVM) was integrated with error correcting output coding (ECOC). ECOC use multiple binary sub-class problems to convert into multiclass problems. The results of binary classes are combined to predict the class of a new sample. This approach was pioneered by Sejnowski and Rosenberg in their widely known NETtalk system (Xiao-Feng et al., 2010)

2.2.3 Classification models and performance metrics

The performances of the three selected classification methods were evaluated and compared in terms of false-color classified images for both the training and the validation sets and in terms of statistical parameters: Sensitivity, Specificity and Efficiency. Sensitivity expresses the model ability to correctly recognize samples belonging to the considered class and is defined by Equation 2, in which TP represents the total number of True Positive and FN the total number of False Negative. Specificity describes the models ability to correctly reject samples belonging to all the other classes and is defined by Equation 3, in which TN represents the total number of True Negative and FP the total number of False Positive. Both Sensitivity and Specificity can assume values between 0 and 1, the latter being the ideal value for a prediction model. Starting from the two previous mentioned parameters, Efficiency can be calculated, as the geometric mean of Sensitivity and Specificity (Equation 4).

$$Sensitivity = \frac{\text{TP}}{(\text{TP+FN})} \qquad (2)$$

$$Specificity = \frac{\text{TN}}{(\text{TN+FP})} \qquad (3)$$

$$Efficiency = \sqrt{(Sensitivity * Specificity)} \qquad (4)$$

Sensitivity and Specificity were calculated for each developed classification model, based on the correctly/not correctly assigned pixel to each predetermined class, regarding the calibration (CAL) and cross-validation (CV) of the training set, and to the prediction of the validation set (Pred). Efficiency was calculated for the prediction (Pred) of the validation set.

2.2.4 Micro-XRF equipment

Micro-XRF tests were carried out at the Raw Materials Laboratory (RawMaLab) of the Department of Chemical Engineering, Materials & Environment (Sapienza - University of Rome, Italy). Micro-XRF was utilized to confirm the obtained result by HSI device. A benchtop spectrometer (M4 Tornado, Bruker®) equipped with an Rh tube, operating at 50 kV, 200 µA, with 25 µm spot, was used for analysis. Mapping acquisition conditions are 10 ms/pixel and step size 30 µm in vacuum condition at 20 mBar. The analysis of the elements, in particular Na, Si, Fe and Mg, allowed to

map the distribution of asbestos fibers and were then compared with those obtained by HSI based PLS-DA, CART and ECOC-SVM classification.

3. EXPERIMENTAL RESULTS AND DISCUSSION

3.1 Exploratory data analysis

The average and the preprocessed reflectance spectra of the four classes of materials are reported in Figure 3. As reported in Figure 3a, amosite shows absorptions at 1195 and 1415 nm related to the presence of hydroxyl group (OH—) of 3rd and 2nd overtone regions. Low absorptions are also detected in the wavelength region between 1742 and 1974 nm related to OH— group of 1st overtone. The absorption from 2280 to 2343 nm shows characteristic frequencies related to Fe-OH presence. Chrysotile shows two strong and characteristic absorptions at 1220 and 1396 nm due to hydroxyl group (OH—) of 3rd and 2nd overtone region, absorption from 1742 to 1980 nm attributed to OH— of 1st overtone region and, finally, a strong absorption around 2300 nm, attributed to hydroxyl combination band of Mg-OH (Cheng et al., 2017) Crocidolite shows absorptions at 1415 and 1930 nm related to a hydroxyl group (OH—) of 2nd and 1st overtone region, respectively, and absorptions at 2299 and 2336 nm, related to the hydroxyl group of combination band, overlapping with octahedral sites containing ferric iron. Matrix without asbestos shows absorptions at 1220, 1422, 1736, 1774, 2318 and 2355 nm related to the OH— group of natural fiber and organic components that make up the sample. The applied spectra pre-processing (Figure 3b) was: Multiplicative Scatter Correction (MSC) primarily utilized to reduce scattering effects, followed by a 1st Derivative applied to enhance absorption and additive effects, and, finally, by Mean Centering (MC) applied to remove the mean value from the data and to further enhance differences among samples. The entire dataset was thus analyzed by PCA in order to evaluate the spectral features and variability of the four classes.

PCA model requires 3 PCs to obtain the reliable total captured variance of 96.48%. In particular, PC1-PC2 score plot (Figure 4a) shows that pixels belonging to the 'amosite' class are mainly concentrated in the 1st quadrant, corresponding to positive values of PC1 and PC2; pixels belonging 'crocidolite' classes occur in different regions of the plot, mainly in the center of score plot. Pixel Belonging to 'Chrysotile' mainly occur in the middle of 3rd and 4th quadrants. Finally, pixels belonging to 'matrix without asbestos' class occur in different regions of the plot, mainly in the 2nd quadrant, corresponding to negative values of PC1 and positive values of PC2. Loading's analysis (Figure 4b) shows as the variations along with the 1st component are around 1000 nm, 1700 nm and 2300 nm. The variations along with the 2nd component are around 1000 nm, 1900 nm and over 2400 nm.

3.2 Comparison of the different classification models in calibration and cross-validation

The results in terms of Sensitivity and Specificity in calibration and cross-validation for the classification models ECOCSVM, PLS-DA and CART are reported in Table 2. All the proposed models (i.e., PLS-DA, CART and ECOC-SVM) show, in calibration and cross validation, similar results with values close to 1.000 in calibration and cross validation. Only the PLS-DA shows a slight variability with values ranging from 0.998 to 1.000. The results in calibrations and cross validation confirm the correct choice of preprocessing to emphasize the spectral features of the data and the spectral representativeness of the pure asbestos samples.

3.3 Comparison of the different classification models in prediction

The obtained prediction map of the validation set for each classifier is reported in Figure 5, whereas the performance metrics of the classification models applied to the validation set are shown in Table 3, in terms of Sensitivity,Specificity and Efficiency.

PLS-DA. The prediction map (Figure 5b) shows that the 'matrix without asbestos' class is perfectly predicted, whereas the other classes show some pixels incorrectly assigned. In more detail, the main misclassification errors
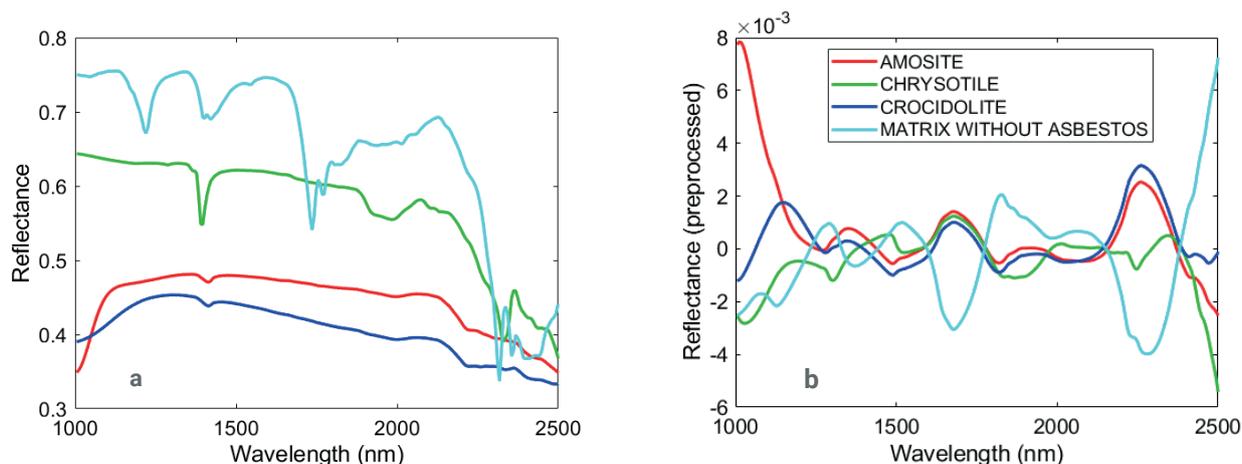

FIGURE 3: Average raw (a) and preprocessed (b) spectra of the different classes selected as results of PCA application to samples constituting the calibration data set.
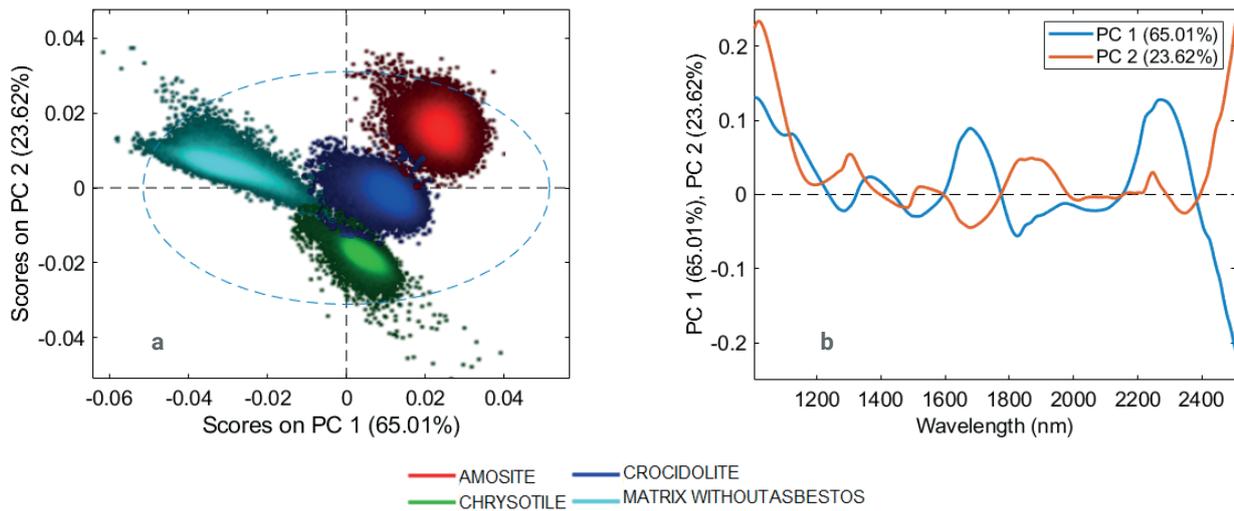
FIGURE 4: PCA score plot (a) and loading plot (b) were utilized to perform data calibration according to the spectral difference detected for each sample.

are among 'amosite and 'crocidolite'. The main misclassified pixels are along the edge of the analyzed samples.

CART. The prediction image resulting from the CART (Figure 5c) model was not as good as expected from the calibration phase, being slightly worse than those obtained by PLS-DA and ECOC-SVM. The class: "matrix without asbestos" is properly identified by the CART model with some misclassified pixels. The main error was in the borders of amosite and chrysotile, that were wrongly assigned to crocidolite.

ECOC-SVM. The prediction map (Figure 5d) shows that the class: "matrix without asbestos" is perfectly predicted, whereas the other classes show some pixels incorrectly assigned. In more detail, the main misclassification errors occur among "amosite" and "crocidolite. The main misclassified pixels are those along the edge of the analyzed samples. Compared to the parametric performances detected in calibration and cross validation, the prediction values show some differences between the 3 classification pro-

posed models. In detail, by analyzing the Efficiency of the 3 models, it is possible to highlight for the PLS-DA a slightly better predictive capacity for the amosite compared to the Efficiency results detected for CART and ECOC-SVM. The best performances in terms of Efficiency for chrysotile detection have been obtained by ECOC-SVM compared to CART and PLS-DA. The best Efficiency in detecting crocidolite is obtained from the ECOC-SVM model followed by PLS-DA and CART. Finally, the matrix without asbestos shows similar values between the three models highlighting an equal performance of the 3 classification models considered. Analyzing the average Efficiency values, the best performances are obtained from the ECOC-SVM model with values close to 1 (0.985) followed by PLS-DA (0.943) and CART (0.935) which show average Efficiency values very close to each other. To confirm the absence of chrysotile, crocidolite and amosite in the sample named "matrix without asbestos" and to verify the quality of the

TABLE 2: Sensitivity and Specificity in calibration (Cal) and cross-validation (CV) of PLS-DA, CART and ECOC-SVM.

PLS-DA	Amosite	Chrysotile	Crocidolite	Matrix without asbestos
Sensitivity (Cal):	1,000	0,999	0,999	1,000
Specificity (Cal):	1,000	1,000	0,989	0,998
Sensitivity (CV):	1,000	0,999	0,999	1,000
Specificity (CV):	1,000	1,000	0,976	0,998
Cart	**Amosite**	**Chrysotile**	**Crocidolite**	**Matrix without asbestos**
Sensitivity (Cal):	1,000	1,000	1,000	1,000
Specificity (Cal):	1,000	1,000	1,000	1,000
Sensitivity (CV):	1,000	1,000	1,000	1,000
Specificity (CV):	1,000	1,000	1,000	1,000
ECOC-SVM	**Amosite**	**Chrysotile**	**Crocidolite**	**Matrix without asbestos**
Sensitivity (Cal):	1,000	1,000	1,000	1,000
Specificity (Cal):	1,000	1,000	1,000	1,000
Sensitivity (CV):	0,999	1,000	1.000	1,000
Specificity (CV):	1,000	1,000	1,000	1,000

TABLE 3: Sensitivity, Specificity and Efficiency in prediction (PRED) of PLS-DA, CART and ECOC-SVM.

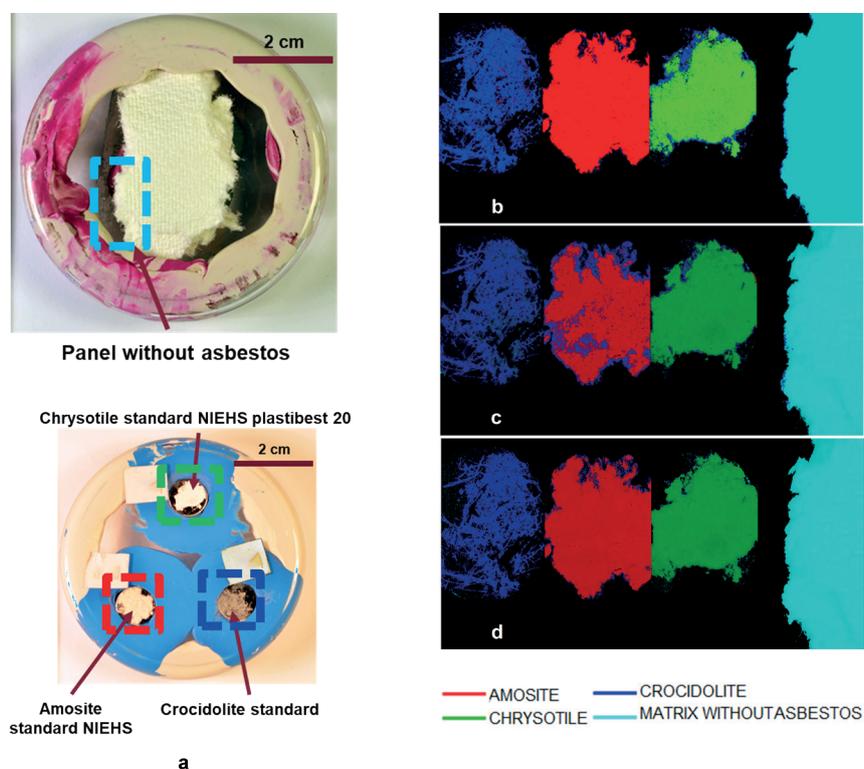| PLS-DA	Amosite	Chrysotile	Crocidolite	Matrix without asbestos
Sensitivity (Pred):	0.969	0,819	0,902	1,000
Specificity (Pred):	0,996	1,000	0,969	0,900
Efficiency	0,982	0,905	0,935	0,949
Cart	**Amosite**	**Chrysotile**	**Crocidolite**	**Matrix without asbestos**
Sensitivity (Pred):	0,994	0,944	0,689	0,993
Specificity (Pred):	0,925	0,983	0,984	0,998
Efficiency	0,959	0,963	0,823	0,995
ECOC-SVM	**Amosite**	**Chrysotile**	**Crocidolite**	**Matrix without asbestos**
Sensitivity (Pred):	0,945	0,977	0,989	1,000
Specificity (Pred):	1,000	1,000	0,979	0,993
Efficiency	0,972	0,988	0,984	0,996
PLS-DA	**Amosite**	**Chrysotile**	**Crocidolite**	**Matrix without asbestos**
Sensitivity (Pred):	0,969	0,819	0,902	1,000
Specificity (Pred):	0,996	1,000	0,969	0,900
Efficiency	0,982	0,905	0,935	0,949
Cart	**Amosite**	**Chrysotile**	**Crocidolite**	**Matrix without asbestos**
Sensitivity (Pred):	0,994	0,944	0,689	0,993
Specificity (Pred):	0,925	0,983	0,984	0,998
Efficiency	0,959	0,963	0,823	0,995
ECOC-SVM	**Amosite**	**Chrysotile**	**Crocidolite**	**Matrix without asbestos**
Sensitivity (Pred):	0,945	0,977	0,989	1,000
Specificity (Pred):	1,000	1,000	0,979	0,993
Efficiency	0,972	0,988	0,984	0,996

FIGURE 5: Digital image of the validation set (a) Prediction maps were obtained applying the developed PLS-DA (b) and CART (c) and ECOC-SVM(d) classifier.

pure asbestos fibers used for the calibration and prediction set, elements maps of the samples were made (Figure 6 and Table 4). The chrysotile maps are mainly characterized by the presence of magnesium distributed over the whole sample. Crocidolite and amosite are characterized by the presence of iron; however, sodium is also present only in crocidolite and not in amosite. The asbestos-free matrix has a totally different composition mainly characterized by the presence of iron, potassium and titanium. Silicon is present in all pure asbestos fibers considered. Regarding iron inside matrix without asbestos, the concentration is relatively low and no asbestiform forms are detected. The distribution maps obtained, confirm the presence of the main detectable elements in pure fibers and as a consequence validate the correct prediction obtained from the 3 classification models proposed.

The proposed methodological approach highlights how theoretically it is possible to achieve an accuracy very close to 1 in laboratory conditions. However, in order to extract the maximum information useful for the classification, the statistical method to be used becomes crucial in order to minimize the error in classification. The results of this work clearly demonstrate as SWIR hyperspectral spectroscopy is potentially the most powerful technique for the rapid, accurate and reliable detection and identification of ACM utilized in the construction sector. Finally, the reduction of HSI hardware costs combined with increased processing power and speed could dramatically contribute to push the utilization of this technique in asbestos and/or ACM contaminated areas, also reducing workers risks (Serranti et al., 2020).
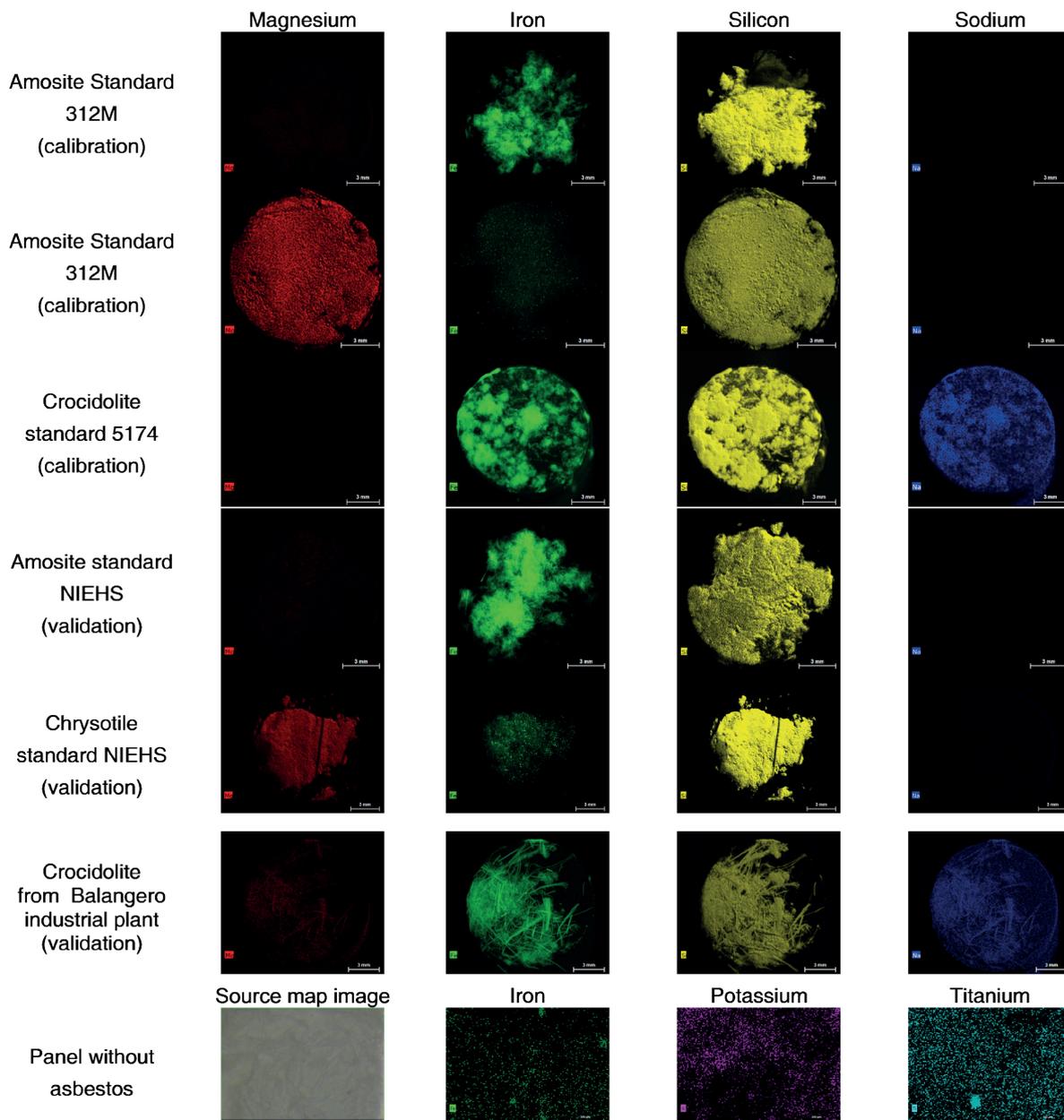

FIGURE 6: Elemental maps as resulting from the micro-XRF analysis carried out on samples.

TABLE 4: Elements concentration of the pure asbestos fibers expressed in normalized mass percent (wt%) assumed as a reference for the calibration and validation test and those resulting from the panel without asbestos.

Spectrum	Na	Mg	Si	S	Cl	K	Ca	Ti	Mn	Fe	Zn
Amosite Standard 312M		0,94	34,49						4,55	60,02	
Crocidolite standard 5174	0,92	2,95	56,42							39,71	
Chrysotile standard intermediate 031G		34,48	65,52								
Panel without asbestos			3,93	10,37	10,14	6,64	64,45	0,47		0,72	3,28
Chrysotile standard NIEHS plastibest 20		34,66	65,34								
Amosite standard NIEHS		2,02	30,65						5,74	61,59	
Crocidolite from Balangero industrial plant	2,15	3,11	56,81							37,92	

4. CONCLUSIONS

In the present study, three different classification models (i.e. PLS-DA, CART and ECOC-SVM) based on SWIR hyperspectral imaging, were applied and compared to define the most accurate and reliable strategy for the automatic detection of different types of asbestos fibers (i.e.: chrysotile, crocidolite and amosite) from the matrix without asbestos. Different goals were achieved:

- The data structures, related to the hyperspectral attributes of each sample (i.e., hypercubes), were processed through a multivariate statistical analysis, starting from a spectral database referred to pure asbestos samples, taken as a reference. The distinction was made between three types of asbestos, (i.e., amosite, chrysotile, crocidolite) and a fibrous matrix without asbestos. The distinction was carried out through the collection and processing of their hyperspectral attributes acquired in the SWIR region (1000−2500 nm).
- Three different classification models were developed (i.e., PLS-DA, CART, ECOC-SVM) in order to evaluate the best methodological approach to identify different type of fibers at the same time with a low value of false positive. Despite the average Efficiency of each classification model is higher (the minimum value was obtained for for crocidolite with CART and corresponding to 0.823), the experimental results in prediction demonstrated that the ECOC-SVM, thanks to the capability to extract nonlinearly features, has the best identification accuracy,.
- The elemental maps obtained by micro-Xray fluorescence, showing the average distribution of the elements in pure asbestos and the absence of asbestos fibers in white fibrous panel, confirm the results and quality of prediction in laboratory scale.

Furthermore, this technique, moreover, does not require direct contact and combining with a classification approach the presence of an expert operator is not necessary. Despite the good results obtained with this methodology it is important to highlight that, the texture of C&DW materials can significantly impact the Efficiency in asbestos recognition. The high variability of constituting construction and demolition waste materials also requires spectral libraries updating, and a correspondent model tuning, to correctly assess material characteristics and to perform their sorting.

Further studies will be addressed to compare different matrix types and to adopt more complex classifiers, able to take into account several possible scenarios where HSI sensing units can be profitably utilized for asbestos recognition "in situ", leading to a reduction in costs and analysis time.

Thanks to the continuous technological implementations of miniaturized scanning systems, in the next future further advantages could also be envisaged in the use of these methods for the characterization of aggregates/waste, including those coming from disasters.

AKNOWLEDGEMENTS

REFERENCES

Allen, L. P., Baez, J., Stern, M. E. C., Takahashi, K., & George, F.m., (2018). Trends and the economic effect of asbestos bans and decline in asbestos consumption and production worldwide. International journal of environmental research and public health, 15(3), 531. https://doi.org/10.3390/ijerph15030531

Amigo, J. M., Martí, I., & Gowen, A., (2013). Hyperspectral imaging and chemometrics: a perfect combination for the analysis of food structure, composition and quality. Data handl. Sci., 28, 343-370. In Data handling in science and technology (Vol. 28, pp. 343-370). https://doi.org/10.1016/B978-0-444-59528-7.00009-0

Ballabio, D., & Consonni, V., (2013). Classification tools in chemistry. Part 1: linear models. PLS-DA. Analytical Methods, 5(16), 3790-3798. https://doi.org/10.1039/C3AY40582F

Bonifazi, G., Capobianco, G., & Serranti, S., (2018). A hierarchical classification approach for recognition of low-density (LDPE) and high-density polyethylene (HDPE) in mixed plastic waste based on short-wave infrared (SWIR) hyperspectral imaging. Spectrochim. Acta A, 198, 115-122. https://doi.org/10.1016/j.saa.2018.03.006

Bonifazi, G., Capobianco, G., & Serranti, S., (2018). Asbestos containing materials detection and classification by the use of hyperspectral imaging. J. hazard. Mate., 344, 981-993. https://doi.org/10.1016/j.jhazmat.2017.11.056

Bonifazi, G., Capobianco, G., & Serranti, S., (2019). Hyperspectral Imaging and Hierarchical PLS-DA Applied to Asbestos Recognition in Construction and Demolition Waste. Applied Sciences, 9(21), 4587. https://doi.org/10.3390/app9214587

Bonifazi, G., Capobianco, G., Gasbarrone, R., & Serranti, S., (2021). Contaminant detection in pistachio nuts by different classification methods applied to short-wave infrared hyperspectral images. Food Control, 108202. https://doi.org/10.1016/j.foodcont.2021.108202

Bonifazi, G., Capobianco, G., Palmieri, R., & Serranti, S., (2019). Hyperspectral imaging applied to the waste recycling sector. Spectrosc. Eur., 31, 8-11.

Bonifazi, G., Palmieri, R., & Serranti, S., (2018). Evaluation of attached mortar on recycled concrete aggregates by hyperspectral imaging. Constr. build. mater., 169, 835-842. https://doi.org/10.1016/j.conbuildmat.2018.03.048

Bro, R., & Smilde, A. K., (2014). Principal component analysis. Analytical methods, 6(9), 2812-2831. DOI: 10.1039/C3AY41907J

Chapelle, O., Haffner, P., & Vapnik, V. N., (1999). Support vector machines for histogram-based image classification. IEEE transactions on Neural Networks, 10(5), 1055-1064. DOI: 10.1109/72.788646

Cheng, H., Hao, R., Zhou, Y., & Frost, R. L. (2017). Visible and near-infrared spectroscopic comparison of five phyllosilicate mineral samples. Spectrochim. acta a, 180, 19-22. https://doi.org/10.1016/j.saa.2017.02.043

Colangelo, F., Cioffi, R., Lavorgna, M., Verdolotti, L., & De Stefano, L., (2011). Treatment and recycling of asbestos-cement containing waste. J. hazard. Mate., 195, 391-397. https://doi.org/10.1016/j.jhazmat.2011.08.057

Deconinck, E., Sacré, P. Y., Coomans, D., & De Beer, J. (2012). Classification trees based on infrared spectroscopic data to discriminate between genuine and counterfeit medicines. J. pharmaceut. biomed., 57, 68-75. https://doi.org/10.1016/j.jpba.2011.08.036

Eigenvector Inc, Get organized with dataset object https://eigenvector.com/software/dataset-object/ (2021), Accessed 30 November 2021

Gandolfi, N. B., Gualtieri, A. F., Pollastri, S., Tibaldi, E., & Belpoggi, F. (2016). Assessment of asbestos body formation by high resolution FEG−SEM after exposure of Sprague−Dawley rats to chrysotile, crocidolite, or erionite. J. hazard. Mate., 306, 95-104. https://doi.org/10.1016/j.jhazmat.2015.11.050

Grahn, H., & Geladi, P., (Eds.). (2007). Techniques and applications of hyperspectral image analysis. John Wiley & Sons. ISBN: 978-0-470-01086-0

Gualtieri, A. F., (2020). Naturally occurring asbestos: A global health concern? State of the art and open issues. Environmental & Engineering Geoscience, 26(1), 3-8. https://doi.org/10.2113/EEG-2271

Neo, E. R. K., Yeo, Z., Low, J. S. C., Goodship, V., & Debattista, K. (2022). A review on chemometric techniques with infrared, Raman and laser-induced breakdown spectroscopy for sorting plastic waste in the recycling industry. Resources, Conservation and Recycling, 180, 106217. https://doi.org/10.1016/j.resconrec.2022.106217

Petriglieri, J. R., Salvioli-Mariani, E., Mantovani, L., Tribaudino, M., Lottici, P. P., Laporte-Magoni, C., & Bersani, D., (2015). Micro-Raman mapping of the polymorphs of serpentine. J. Raman Spectrosc., 46(10), 953-958. https://doi.org/10.1002/jrs.4695

Rinnan, Å., Van Den Berg, F., & Engelsen, S. B., (2009). Review of the most common pre-processing techniques for near-infrared spectra. TrAC Trends in Analytical Chemistry, 28(10), 1201-1222. https://doi.org/10.1016/j.trac.2009.07.007

Satapathy, S. K., Dehuri, S., Jagadev, A. K., & Mishra, S. (2019). EEG Brain Signal Classification for Epileptic Seizure Disorder Detection. Academic Press,. Elsevier. ISBN: 9780128174272

Serranti, S., & Bonifazi, G. (2016, April). Hyperspectral imaging and its applications. In Optical Sensing and Detection IV (Vol. 9899, p. 98990P). International Society for Optics and Photonics. https://doi.org/10.1117/12.2234976

Serranti, S., & Bonifazi, G. (2020). Detection and classification of asbestos and other contaminants in C&DW by advanced technologies. In Advances in Construction and Demolition Waste Recycling (pp. 407-437). Woodhead Publishing. https://doi.org/10.1016/B978-0-12-819055-5.00020-6

Serranti, S., Bonifazi, G., Capobianco, G., Malinconico, S., & Paglietti, F. (2019, May). Hyperspectral imaging applied to asbestos containing materials detection: specimen preparation and handling. In Advanced Environmental, Chemical, and Biological Sensing Technologies XV (Vol. 11007, p. 110070S). International Society for Optics and Photonics. Baltimore, Maryland, United States. https://doi.org/10.1117/12.2517070

Specim Hyperspectral - instruments Sisuchema X.L https://www.specim.fi/wp-content/uploads/2020/03/SisuCHEMA_2_2015.pdf (2015), Accessed 30 November 2021

Stănescu-Dumitru, R. (2008). FTIR asbestos presence identification in the occupational environment. Analele UniversităŃii din Bucureşti – Chimie, Anul XVII (serie nouă), vol. II, pag. 79 – 83spectroscopy, 4, 6.

The National Institute for Occupational Safety and Health (NIOSH) NIOSH (2008). Current Intelligence Bulletin (January 20, 2009) June 2008-Revised Draft) Asbestos and Other Elongated Mineral Particles: State of the Science and Roadmap for Research. https://www.cdc.gov/niosh/docket/archive/pdfs/NIOSH-099b/099B-040109AsbestosNAReviewDoc.pß

Tomassetti, L., Di Giuseppe, D., Zoboli, A., Paolini, V., Torre, M., Paris, E., E., Guerriero, F., Petracchini & Gualtieri, A. F., (2020). Emission of fibres and atmospheric pollutants from the thermal treatment of asbestos containing waste (ACW). Journal of Cleaner Production, 268, 122179. https://doi.org/10.1016/j.jclepro.2020.122179

Trotta, O., Bonifazi, G., Capobianco, G., & Serranti, S., (2021). Recycling-Oriented Characterization of Post-Earthquake Building Waste by Different Sensing Techniques. Journal of Imaging, 7(9), 182. https://doi.org/10.3390/jimaging7090182

Wise, B. M., Gallagher, N. B., Bro, R., Shaver, J. M., Windig, W., & Koch, R. S., (2006). Chemometrics tutorial for PLS_toolbox and solo. Eigenvector Research. Inc., Wenatchee, Washington.

World Health Organization. Asbestos: elimination of asbestos-related diseases. https://www.who.int/news-room/fact-sheets/detail/asbestos-elimination-of-asbestos-related-diseases. Published February 15, 2018. Accessed May 03, 2022.

Xiao-Feng, L., Xue-ying, Z., & Ji-Kang, D., (2010, September). Speech recognition based on support vector machine and error correcting output codes. In 2010 First International Conference on Pervasive Computing, Signal Processing and Applications (pp. 336-339). IEEE. DOI: 10.1109/PCSPA.2010.88IEEE

Zheng, G., Qian, Z., Yang, Q., Wei, C., Xie, L., Zhu, Y., & Li, Y., (2008). The combination approach of SVM and ECOC for powerful identification and classification of transcription factor. BMC bioinformatics, 9(1), 1-8. doi:10.1186/1471-2105-9-282

Zholobenko, V., Rutten, F., Zholobenko, A., & Holmes, A. (2021). In situ spectroscopic identification of the six types of asbestos. J. hazard. Mate., 403, 123951. https://doi.org/10.1016/j.jhazmat.2020.123951